Effective Polarization in Potassium Channel Simulations: Ion Conductance, Occupancy, Voltage Response, and Selectivity

Chenggong Hui[1], Reinier de Vries[1], Wojciech Kopec[1,2]*, Bert L. de Groot[1]*

[1]Computational Biomolecular Dynamics Group, Max Planck Institute for Multidisciplinary Sciences, Am Fassberg 11, 37077 Göttingen, Germany

[2]Department of Chemistry, Queen Mary University of London, 327 Mile End Road, London E1 4NS, United Kingdom

*corresponding authors: w.kopec@qmul.ac.uk, bgroot@gwdg.de

Classification : Biological Science, Biophysics and Computational Biology

Keywords : Potassium Channel, MD simulation, Force Field, Charge Scaling, Selectivity

Significance Statement

Potassium (K^+) channels are essential membrane proteins that facilitate the selective conduction of K^+ ions while excluding Na^+ ions. Incorporation of electronic polarization effects through the Electronic Continuum Correction (ECC) method enables molecular dynamics simulations to reproduce rapid K^+ permeation under physiological voltage conditions. In this study, we demonstrate that employing ECC approximated polarization in molecular dynamics simulations allows for the prediction of multiple channel properties: conductance, ion occupancy, voltage response, and selectivity, with unprecedented accuracy. Furthermore, our simulations provide atomistic insights into the asymmetrical current-voltage (I-V) relationship observed in the MthK channel.

Abstract

Potassium (K^+) channels are widely distributed in many types of organisms. They combine high efficiency (~100 pS) and K^+/Na^+ selectivity by a conserved selectivity filter (SF). Molecular Dynamics (MD) simulations can provide detailed, atomistic mechanisms of this sophisticated ion permeation. However, currently there are clear inconsistencies between computational predictions and experimental results. Firstly, the ion occupancy of the SF in simulations is lower than expected (~2.5 in MD compared to ~4 in X-ray crystallography). Secondly, in many reported MD simulations of K^+ channels, K^+ conductance is typically an order of magnitude lower than experimental values. This discrepancy is in part because the force fields used in MD simulations of potassium channels do not account for polarization. One of the proposed solutions is the Electronic Continuum Correction (ECC), a force field modification that scales down formal charges, to introduce the polarization in a mean-field way. When the ECC is used in conjunction with the Charmm36m force field, the simulated K^+ conductance increases 13-fold. Following the analysis of ion occupancy states using Hamiltonian Replica Exchange (HRE) simulations, we propose a new parameter set for Amber14sb, that also leads to a similar increase in conductance. These two force fields are then used to compute, for the first time, the full current-voltage (I-V) curves from MD simulations, approaching quantitative agreement with experiments at all voltages.

In general, the ECC-enabled simulations are in excellent agreement with experiment, in terms of ion occupancy, conductance, current-voltage response, and K^+/Na^+ selectivity.

1. Introduction

Potassium channels play an important role in many cell types. They set the resting potential in non-excitable cells or reset the potential in depolarization in excitable cells. Potassium channels are known for their efficient and selective permeation of potassium ions. For instance, the NaK2K channel conducts Na^+ ions at ~10 pS in NaCl solution while conducting K^+ ions at 120 pS in KCl solution.[1] All potassium channels share a conserved selectivity filter (SF), which forms 4 adjacent ion binding sites made of backbone carbonyl oxygens (sites S1-S3), plus typically 4 threonine hydroxyl oxygens at the S4 site. When the high-resolution crystal structure of KcsA was first published[2], the electron density in the 4 binding sites was initially interpreted as two K^+ ions occupying two non-adjacent binding sites and two water molecules placed in between the ions. This interpretation suggests that the four peaks in the electron density represent an overlap of two distinct states: K^+-water-K^+-water and water-K^+-water-K^+.[3] Consequently, the hypothesis of a water-mediated "soft knock-on" permeation mechanism was coined. More recent anomalous X-ray diffraction studies in NaK2K and KcsA channels suggested that all of the 4 sites are fully occupied by K^+ ions,[4–6] which supports an alternative hypothesis of direct knock-on mechanism, observed in numerous Molecular Dynamics (MD) studies,[7–10] that does not include any co-permeation of water. A more detailed discussion can be found in our recent review.[11]

Despite the debated permeation mechanism, low conductance and low K^+ occupancy of the binding sites were consistently observed in MD simulations of potassium channels displaying both soft and direct knock-on mechanisms, although direct knock-on typically results in higher conductance[7,12]. In our previous work, direct knock-on was observed during continuous permeation under membrane voltage, with the SF typically containing 2 or 3 ions.[7] Specifically, spontaneous permeation under voltage has been observed on MthK, KcsA, NaK2K, BK, Kv1.2, TREK2, and TRAAK,[8,13,14] but the conductance was generally one order of magnitude lower than the experimental values. Ion occupancy in the SF, permeation mechanism, and conductance in MD

simulations all eventually result from a subtle balance of various interactions between ions, protein, and water. Even tiny changes in the interaction parameters between them might change the kinetics, thermodynamics, and mechanism of ion permeation.

One often discussed cause for the observed shortcomings in current simulations of K^+ channels is the lack of explicit electronic polarization in classical force fields.[15] In a classical, fixed-charged force field (e.g. Amber, Charmm, OPLS-AA), atoms are modeled as spheres (particles) with assigned partial charges, as an approximation of positively charged nuclei with clouds of electrons around them. In MD simulations, electrostatic interactions are computed between these particles by applying the Coulomb law and using the dielectric constant of vacuum. In reality however, the electrostatic interactions between the nuclei will be (differently) screened by the instantaneous distribution of the electrons, that will be in turn affected by the position of the nuclei (i.e. electronic polarization), resulting in the relative permittivity >1. Therefore, for the more accurate modeling of electrostatic interactions, two general solutions have been proposed. In the first one, force fields with explicit electronic polarization are developed, whereas in the second one, the so-called Electronic Continuum Correction (ECC) is applied to existing, classical force fields. Ren and coworkers have tested both solutions in MD simulations of a K^+ channel[16], focusing on the different K^+ occupancy states of the SF. They found that when the ECC is applied, Charmm36m behaves similarly to the AMOEBA polarizable force field, and both show the SF being fully occupied with four K^+ ions to be energetically the most stable configuration. In practice, the ECC is achieved by rescaling the formal partial charges of ionized groups (such as side chains of arginine, lysine, glutamine, and aspartate amino acids) and ions, which is mathematically the same as changing the dielectric constant in computing electrostatic interactions via Coulomb law.[17,18] This approach has been recently applied to improve force fields for ions, proteins, and lipids.[19–23] In general, the argument is made that the rescaling factor should be ~sqrt(1/2) ≈ 0.7, because the electronic screening factor (high-frequency dielectric constant) is about 2 for most organic media.[24] However, there are at least two reasons why directly applying this number might not be optimal. First, the exact dielectric constant of the approximated medium between MD particles is not known and might be system-dependent. Our main interest here is the magnitude of channel conductance and corresponding free energy difference between relevant SF occupancies. Second, most of the force field parameters were developed without ECC in mind, and might compensate

for the mean polarization to some extent. Therefore, instead of focusing on a single scaling factor, in this work, we combine the ECC approach with two common fixed-charge force fields: Charmm36m and Amber14sb, at various scaling factors (1.0-0.65), to study ion permeation in three different potassium channels. We carefully developed new Lennard-Jones (LJ) parameters, describing van der Waals (vdW) interactions, at each scaling factor, so that the ion radius and solvation free energy are consistent with the original force field. We observe that the ECC dramatically increases the simulated conductance in Charmm36m, to a level that quantitatively agrees with the experimental single-channel conductance. In contrast, the ECC has only a minor effect with the Amber14sb force field. These discrepancies are rationalized using Hamiltonian Replica Exchange (HRE) simulations, providing insights into the effect of the ECC on the SF ion occupancy, and resulting in adjusted SF partial charges for Amber14sb, which consequently predicts conductance close to the experiments as well. We further apply these force fields in simulations under physiological voltage <-150, +150 mV>, recording, for the first time, full I-V curves, compatible with experiments. The K^+/Na^+ selectivity is preserved, indicating the necessity of adjusting LJ parameters of ions in ECC. Finally, applying the recently introduced permeation cycle analysis, we provide cues into the physical basis of inward rectification in the MthK channel.

2. Results and Discussion

2.1. Low conductance and SF occupancy in MD with Charmm36m and Amber14sb force fields

To obtain a comprehensive view on ion permeation in K^+ channels, we simulated three different channels, namely NaK2K, TRAAK, and MthK. Whereas the archaeal MthK channel shares the SF sequence (TVGYGD) with the NaK-derived NaK2K channel, the SF sequence of TRAAK is more varied: being a dimer, TRAAK has two SF strands (called SF1) with a TIGYGN sequence, and two with TVGFGD (SF2). The inclusion of TRAAK simulations allows us to generalize our findings beyond the most common SF sequence. The channels were simulated using both the Charmm36m and Amber14sb force fields. When compared with experiments, a clear discrepancy in quantities describing ion permeation, such as conductance and SF occupancy is seen, as previously reported by us and others.[7–9,13] Generally speaking, single channel conductance (Fig.

137 1a) is underestimated by an order of magnitude in all channels and force fields tested. The
138 instantaneous occupancy of the SF binding sites during permeation (Fig. 1b) predominantly shows
139 (despite differences between force fields, Table S1) an alternation between 3-ion and 2-ion
140 (counting ions in S1 to S4) SF occupancy states. Although this quantity is not readily available
141 from experiments, and the SF occupancy during permeation is debated (see Introduction), we note
142 here that the 3-ion and 2-ion states underestimate the possible number of ions in the SF, as
143 compared to anomalous diffraction data (full SF occupancy in S1-S4 at 100 K and 3.44 total
144 occupancy at 292 K).[4,25] These results clearly show the need for improved force fields for MD
145 simulations of K^+ channels. Efforts have been made in this direction. For example a special
146 exception interaction (NBFIX) was developed to weaken the interaction between carbonyl
147 oxygens and K^+ ions,[26] but reproducing the conductance was found to be challenging.[27] We reason
148 that single channel potassium conductance is the central quantity describing ion permeation, which
149 can be directly compared between simulations and experiments. Therefore, an improved force field
150 should predict the single channel conductance close to the experimental value, across the same
151 voltage range as used in electrophysiology (-150 ~ 150 mV), and ideally also in the physiological
152 range (resting potential: -10 ~ -100 mV, action potential: ~+100 mV).[28,29] We further reason that
153 such a force field would likely better describe any secondary observables characterizing ion
154 permeation (i.e. SF occupancy states, rate limit steps, SF geometries etc.) as well.
155

156 In this contribution, we show how the ECC-introduced polarization in Charmm36m and
157 Amber14sb force fields improves simulated single channel conductance in all channels tested.
158 Interestingly, the application of charge scaling simultaneously results in SFs occupied by more K^+
159 ions (3-ion and 4-ion states) than in non-scaled force fields, agreeing well with experimental data,
160 and further highlighting the role of direct ion-ion contact in rapid K^+ permeation through K^+
161 channels.

162

163 ## 2.2. ECC-Charmm36m improves the conductance, but ECC-Amber does not.

164 We performed simulations with different scaling factors, starting at the nominal charge of +1.0,
165 with a step of 0.05, down to +0.65, in Charmm36m and Amber14sb. Similarly to simulations with

166 unscaled charges, we initially used an applied voltage of +150 mV to drive ion permeation. The
167 conductance at different levels of ECC (scaling factors) in the NaK2K channel is shown in Fig.
168 2a-c (see Fig. S4 and S5 for TRAAK and MthK channels, respectively). We first focus on
169 simulations using Charmm36m (Fig. 2a, d, g). Compared to the standard parameters (scaling factor
170 of 1.00), the conductance decreases at +0.9 charge, but then significantly increases around ~+0.75.
171 At the scaling factor of 0.75, the conductance is 122.4 ± 10.1 pS, which is a 13-fold increase
172 compared to standard Charmm36m (9.2 ± 1.7 pS), and in apparent excellent agreement with the
173 experimental single channel conductance of ~120 pS.[1] The equilibrated populations of the SF
174 states show major changes with the applied scaling factor. Compared to standard Charmm36m, 4-
175 ion states become gradually more populated with stronger scaling (Fig. 2d, g): the WKKKK0 state
176 is dominant (79%) with 0.7 scaling, in stark contrast to unscaled Charmm36m (WKK0K0 (37%),
177 WK0KK0 (20%), WK0K0K (20%)). The increase of ion occupancy is consistent with the
178 previously reported ECC-Charmm36m simulation in KcsA.[16] A similar effect of increased ion
179 occupancy with charge scaling is observed in Amber14sb (Fig. 2e,h), however there is no effect
180 on conductance, as it remains low (~20 pS) at all scaling factors tested, also in the other two
181 channels (Fig. S4 and S5).

182

183 ## 2.3. Redistributing the charge in the SF in Amber14sb increases the conductance

184 Prompted by the conductance insensitivity to charge scaling in Amber14sb, we decided to
185 investigate this issue in detail. By comparing simulations carried out with Charmm36m and
186 Amber14sb we noticed two important (and possibly related) differences: 1. In Charmm36m, the
187 carbonyl oxygen has a partial charge of -0.51, whereas it is -0.5679 in Amber14sb, potentially
188 resulting in stronger binding of a K^+ ion to the SF, and 2. For the <0.85, 0.75> range of charge
189 scaling in Amber14sb, the K0KKK0 state is the dominant one, and, for scalings < 0.75, WKKKK0
190 dominates (Fig. 2e). These observations suggest that K^+ ions in Amber14sb are potentially too
191 strongly bound to the SF, especially to its lower part, which might slow down permeation. To test
192 this idea, we reduced the negative charge on the carbonyl oxygen atoms at S3 to different values
193 (-0.55, -0.53, -0.51), and evenly distributed the remaining charge on the other atoms in the SF (see
194 Fig S1 for the illustration of oxygen charge in the SF). -0.53 gave the SF state population similar

195 to Charmm36m (see Fig. 2 and Fig. S2 for SF state population). We further tested the -0.53 charge
196 modification and call it Amber14sb-S3 from now on.

197

198 With this modified force field at hand, we repeated all the simulations for all three channels (Fig.
199 2c, f, i, Fig. S4, Fig. S5). Interestingly, the state populations (Fig. 2f and i) are now more similar
200 to ECC-Charmm36m. When compared to the original Amber14sb, the major difference is that the
201 population of K0KKK0 which dominated the distribution at 0.8 (Fig. 2e) is now significantly
202 reduced (Fig. 2f). Importantly, these effects resulted in a major increase in conductance, akin to
203 ECC-Charmm36m (Fig. 2c, maximal conductance at the scaling factor of 0.75: 88.0 ± 3.2 pS). We
204 observe essentially the same behavior in simulations of TRAAK and MthK channels (Fig. S4 and
205 S5).

206

207 To obtain clearer mechanistic insights into the factors governing rapid ion permeation at around
208 0.80-0.75 scaling in both Charmm36m and Amber14sb-S3, we looked again at the populations of
209 SF states, but this time combining states together with the same number of K^+ ions bound to the
210 SF (Fig. 2g-i, Fig. S4, Fig. S5). We find that in high conductance regions, there is a similar
211 population for 3-ion and 4-ion population states (crossing of blue and orange lines), suggesting a
212 smooth (barrierless) free energy landscape between microscopic states (SF occupancies). We
213 hence hypothesize that a balanced (low barrier) free energy surface between multiple 3- and 4-ion
214 states is a prerequisite for efficient, rapid ion permeation through the SF of K^+ channels.
215 Accordingly, if certain states dominate the SF state distribution the permeation cycle would be
216 slowed down by the barrier to leaving this state. For example, in Charmm36m at 0.9, the SF is
217 mostly populated by a single WKK0K0 state, whereas in Amber14sb at 0.8, the SF is mostly
218 populated by K0KKK0. Those extra stable states might contribute to the underestimation of
219 conductance in MD simulations.

220

221 Our proof-of-concept Amber14sb-S3 modification opens up a new degree of freedom for force
222 field development in K^+ channel simulations. The default backbone parameters for the SF in
223 Amber14sb do not yield reasonable conductance, instead they result in an SF being stuck at a
224 certain SF state (e.g. K0KKK0 at 0.8 scale). By a slight modification of a partial charge on the

225 backbone carbonyl oxygen (from -0.5679 e to -0.53 e) at the S3 binding site, we adjusted the
226 relative free energies of SF states resulting in an efficient ion permeation. We do not suggest our
227 applied parameter changes as a general force field patch, but a special parameter set for K^+ channel
228 SF.

229

230 Comparing the conductance-scaling relationship for all three channels (Fig. 2a-c, Fig. S4a-c, Fig.
231 S5a-c), the maximal conductance is observed at remarkably similar scaling factors. In ECC-
232 Charmm36, the conductance for TRAAK and NaK2K reached their maximum at 0.78 and 0.77,
233 whereas for MthK at 0.75. In ECC-Amber14sb-S3, 0.78 for TRAAK, 0.75 for NaK2K and MthK.
234 Similarly, the crossing point of 3-ion and 4-ion state populations appears in high conductance
235 regions for all three channels, following the same order: TRAAK 0.82, NaK2K 0.78, MthK 0.77
236 (Charmm36m, Fig. 2g, Fig. S4, Fig. S5), TRAAK 0.79, NaK2K 0.77, MthK 0.77 (Amber14sb-S3,
237 Fig. 2i, Fig. S4, Fig. S5). These results agree well with our hypothesis that the presence of multiple
238 3- and 4-ion states at similar (balanced) free energy levels is a prerequisite for high conductance
239 in K^+ channels. And also agree with the room temperature anomalous scattering occupancy
240 result.[25]

241

242 ## 2.4. The ECC force fields predict I-V curves in agreement with the experiment

243 Encouraged by the unprecedented increase of the simulated single channel conductance at a single
244 voltage of +150 mV when using ECC-Charmm36 and ECC-Amber14sb-S3, we decided to test
245 these force fields in the whole experimental voltage range. As a result, we obtained, for the first
246 time, the full current-voltage (I-V) curves of K^+ channels derived purely from MD simulations, for
247 experimentally and physiologically relevant voltage ranges (Fig. 3). The ECC correction improves
248 conductance at all voltages tested, bringing simulated currents with the ~0.80-0.75 scaling factors
249 very close to the experimental currents (black traces) for all three channels, and in both force fields.
250 This effect is particularly pronounced for the experimentally relevant voltage range (<-150 mV,
251 +150 mV>), where both outward and inward currents with unscaled charges are very low (blue
252 traces). Notably, in all conditions tested, the rapid ion permeation occurs through some variations
253 of the direct knock-on mechanism, that is without any co-permeating water molecules. Generally,

254 the probability of finding water in SF is very low. (K^+/Water occupancy in SF is listed in Table
255 S3). Similar to our findings in the previous section, the highest conductance at all voltages is
256 enabled by the co-existence of several 3-ion and 4-ion states in the SF with similar populations.

257

258 In some cases, the application of the ECC correction leads to simulated currents that are higher
259 than their experimental counterparts (e.g. MthK in ECC-Charmm36m 0.75 scaling at positive
260 voltages, or TRAAK ECC-Amber14sb-S3 0.80 scaling at all voltages), which, to the best of our
261 knowledge, has never been reported before for any MD simulation. This observation poses a
262 challenge in deciding which scaling factor is the optimal one (for a given force field). In this
263 context, it is worth recalling that the shapes of experimental I-V curves might substantially vary
264 between K^+ channels. For the channels tested here, both NaK2K and TRAAK display linear I-V
265 curves[1,30], whereas MthK shows inward rectification[10]. Taking this into account, we notice that
266 ECC-Charmm36m with the 0.78 scaling factor (Fig. 3 (a-c), green traces) is in best agreement with
267 the experimental data, reproducing well shapes of experimental I-V curves, including the inward
268 rectification phenomenon in MthK. A more complex situation is seen in ECC-Amber14sb-S3.
269 Here, the 0.78 scaling factor (Fig. 3 (d-f), green traces) is in almost perfect agreement with
270 experimental data for MthK, and it also predicts the linear I-V curves for NaK2K and TRAAK,
271 but underestimates the current for Nak2K and TRAAK. These examples show that none of the
272 ECC scaling tested here is ideal, and further reparameterization work is needed to obtain a robust
273 set of parameters applicable to MD of any K^+ channel. The observed differences between studied
274 channels (and also scaling factors) might be rationalized by sequence variations in the selectivity
275 filter and the second layer of residues surrounding the selectivity filter. Indeed, while the SF
276 sequence is highly conserved, the residues around it show a higher degree of variability, likely
277 leading to ion occupancy and conductance changes, due to subtle differences in dynamics and
278 intermolecular interactions. However, these observations remain secondary to the primary effect
279 of the ECC correction, that is the substantial (order of magnitude) increase of the single channel
280 current (conductance), observed in the 0.80-0.75 scaling range, to the level comparable with
281 experimental estimates. Thus our work opens the possibility to use, for the first time, MD
282 simulations of K^+ channels in a quantitative manner to study a wide range of phenomena, using
283 the same observable (the current-voltage relationship) as in electrophysiological experiments.

Our ECC simulations carried out at voltages outside of the experimental range of <-150 mV, +150 mV> provide additional insights. For example, the scaling factor showing the maximal conductance in ECC-Charmm36m for NaK2K at 200 mV appears to be 0.75, and, in the absence of experimental data at this voltage, it could have been deemed optimal. However, simulations at lower positive voltages show that this is not the case. Therefore, we conclude that in the future MD simulations of ion channels should be performed, whenever possible, at experimentally and/or physiologically relevant voltages. High voltages have been traditionally used to speed up ion permeation in MD simulations of K^+ channels,[7,10,13,27] occasionally reaching 500 mV or even 750 mV,[27,31,32] although the effects of such high voltages on the protein structure and the permeation mechanism itself are not clear.[7] With the ECC approach, there does not seem to be a need to use such high voltages anymore, since robust currents are achievable at experimental voltages as well.

Finally, we tested two more channels, Kv1.2-2.1 and KcsA E71A with the optimal parameters for ECC-Charmm36m at 0.78 scaling factor. Good agreement with experimental currents at both +150 mV and -150 mV are observed. (Fig. S7)

2.5. K^+/Na^+ selectivity is sensitive to both the ion partial charge and LJ parameters

All K^+ channels show exquisite K^+/Na^+ selectivity (>10:1 permeability ratio, i.e. the ratio of conductances in pure K^+ and Na^+ solutions),[1,33] therefore this important characteristic should be captured in simulations as well. In this section, we first present thermodynamic properties of our newly developed radius-corrected LJ parameters for ECC ions (All of the simulation results above were using these radius-corrected LJ parameters). Secondly, we compare ECC K^+ channel simulations with these new parameters versus unmodified LJ parameters, highlighting the importance of compatible ion LJ parameters in ECC force fields.

The straightforward application of the charge scaling procedure in the ECC has a big effect on ion properties in water. Particularly relevant for ion permeation is the radius of an ion, which is

typically carefully checked versus experimental data during the development of ion parameters. When scaling of the charge is applied, cations will have effectively larger radii, due to the reduced interactions of a scaled charge on an ion with the surrounding water molecules (Fig. 4a), thermodynamically leading to an underestimation of the solvation free energies (Fig. 4b, see Methods for the derivation of the solvation free energy scaling in the ECC).

To amend this situation, we developed new radius-corrected LJ parameters for ECC ions. This was done in a way that at any given scaling factor, the radius of the first solvation shell reproduces the radius in the original (not scaled) force field. We decided to choose the original force field as the fitting target rather than the experimental value to: 1. facilitate the comparison with the original force field, and 2. reduce the perturbation to the original force field. As shown in Fig. 4a, our new parameters for K^+ and Na^+ consistently reproduce the originally parametrized radius. Importantly, also solvation free energies of our radius-corrected ECC ions closely follow experimental values (Fig. 4b).

To test the radius-corrected LJ parameters, we performed MD simulations of the same K^+ channels with Na^+ ions at +150 mV at different scaling factors, and compared simulated outward conductance with K^+ conductance and experimental values (Fig. 5, Fig. S14). The unmodified vdW is only used in Fig. 5 (d-e) and Fig. S14 (d-e) for comparison, it is not recommended to use the unmodified vdW in charge scaling simulations.

With our radius-corrected LJ parameters (Fig. 5 a-c, Fig. S14, Fig. 2, Fig. 3), we observe consistently larger K^+ conductances than Na^+ conductances at all scaling factors larger than ~0.7. Specifically, combined with our I-V curves, we deem the scaling factor of 0.78 optimal for current simulations, i.e. it produces I-V curves that qualitatively match experimental ones, and simultaneously provides robust K^+/Na^+ selectivity for all three tested channels (Table 1). In contrast, for a smaller scaling factor (<0.7), all three channels conduct more Na^+ than K^+ ions, which indicates incorrect selectivity. This observation highlights the balance of strong interactions governing ion permeation and selectivity in K^+ channels, leading to the necessity of careful validation of both the scaling factor and LJ parameters of their accurate simulations. We

342 acknowledge that we did not achieve a perfect match for the conductance ratio across all channels
343 (Table 1), but accurately obtaining energy barrier differences to predict the exact ratio may exceed
344 the precision limits of the classical force field. According to the Eyring equation,[34] a 10:1 ratio in
345 permeation rates at 310K corresponds to approximately the 1.4 kcal/mol difference in the barrier
346 height, and the 2.5:1 ratio corresponds to the 0.6 kcal/mol difference.

347

348 In contrast, when the original (unmodified) LJ parameters are used, K^+/Na^+ selectivity is lost in
349 almost all conditions tested (Fig. 5 d-e, Fig. S14). Our results therefore suggest that the adjustment
350 of LJ parameters, and, consequently, maintaining the correct radii of ions, is necessary to capture
351 their proper permeation and selectivity behavior in K^+ channels with the ECC correction, and will
352 be likely relevant in other systems showing significant ion selectivity.

353

354 ## 2.6. Mechanistic Basis of Inward Rectification

355 As a final insight from our ECC simulations, we decided to take a closer look at simulations
356 displaying inward rectification in the MthK channel (ECC-Charmm36m at 0.78 scaling, Fig. 3c,
357 green curve), that is the larger current at negative voltages than at positive ones. This inward
358 rectification is in excellent agreement with experiment (Fig. 3c, black curve). Importantly, this
359 inward rectification is observed, both experimentally and computationally, for the pore domain
360 only (i.e. without the additional intracellular calcium-binding domains), indicating that it is an
361 inherent property of the K^+ permeation mechanism in this channel. To study it in more detail, we
362 applied a recently proposed analysis of ion permeation mechanisms using permeation cycles.[9] We
363 simplified the cycle by lumping together several states when their exchange rate was above a
364 certain cutoff. The comparison of permeation cycles at +150 mV and -150 mV (Fig. 4) reveals that
365 the rate-limiting step at both voltages is the transition between WKKK0K and WKK0KK states
366 (i.e. a K^+ ion transitioning from S4 to S3 sites during outward permeation, and in the opposite
367 direction during inward permeation; while both S1 and S2 remain occupied by K^+ ions). However,
368 the rate (inverse of the mean first passage time) of this transition differs by 3-fold for these two
369 voltages (0.318 ns^{-1} for +150 mV and 0.912 ns^{-1} for -150 mV). Our approach allows finding such
370 rate limiting states in MD simulations of K^+ channels, and thus deciphering the molecular

371 determinants governing the existence of such states, and rectification properties in different K^+
372 channels in general.

373

374 3. Conclusion

375 In this work, we introduced and tested a range of parameters for K^+ and Na^+ ions consistent with
376 the ECC framework, i.e. including effective electronic polarization, in MD simulations of
377 potassium channels. We applied the same methodology to two fundamentally different force fields
378 (Charmm36m and Amber14sb), ran simulations of three different K^+ channels over the whole
379 range of physiologically and experimentally relevant voltages. Despite minor differences between
380 specific cases, our findings can be broadly summarized in three major points: 1. The introduction
381 of the electronic polarization of cations (here through the ECC approach) is crucial to accurately
382 model K^+ ion permeation through potassium channels, allowing to simulate, for the first time, full
383 I-V curves from atomistic MD simulations that are in very good agreement with experimental data;
384 2. This efficient K^+ permeation occurs in all cases through the direct knock-on mechanism, with
385 an even higher number of ions occupying the SF than seen in previous simulations, aided by
386 reduced ion-ion repulsion due to electronic polarization (Fig. 7). Specifically, a highly conductive
387 K^+ channel can accommodate 3 or 4 ions in the SF. Furthermore, achieving balanced free energy
388 between the 3-ion and 4-ion states is crucial for facilitating low barrier permeation (Fig. 7).
389 Consequently, throughout all simulations conducted in this study, virtually no water molecules
390 cross any potassium channels; 3. A careful adjustment of ion LJ parameters is necessary to recover
391 correct ion radii and solvation free energies, which, as we showed, is critical for correct K^+/Na.
392 selectivity in K. channels. We therefore postulate, based on our and other works[4,16], that the
393 conductive state of the SF is characterized by near-full occupancy of K^+ in many conditions.

394

395 In our simulations, the best overall performing force field is CHARMM36m at a scaling factor of
396 0.78 with radius-corrected LJ parameters for ECC ions. This force field correctly reproduces I-V
397 curves in all three channels, as well as their K^+/Na^+ selectivity and inward rectification in the MthK
398 channel. We would therefore recommend it for simulations of other potassium channels, however
399 slight adjustments of the scaling factor might result in a better performance for a specific channel.

Our newly developed parameters allow for MD simulations of K^+ channels at an unprecedented level of accuracy. As almost any process involving K. channels is related to the SF behavior and its occupancy by K^+ ions, we envision future simulation studies to benefit from these findings. Computational insights into the mechanisms of, for example, current regulation, selectivity filter gating or channel modulation by small molecules are now accessible at a much higher accuracy, especially as current readout is now readily accessible at unprecedented accuracy.

4. Methods

4.1. System preparation

4.1.1. NaK2K

The crystal structure 3ouf[1] was used and oriented in the membrane using OPM.[35] 8 water molecules present in the crystal structure, behind the SF of NaK2K, were preserved. The current-increasing F92A mutation[1,36], ACE and NME termini patching, membrane and solvation box building were performed using Charmm-GUI,[37,38] webserver. The final system consisted of one tetrameric channel, 168 POPC molecules, 11,134 water molecules, 160 K^+ ions, 152 Cl^- ions, corresponding to 0.8 m/L salt concentration.

4.1.2. TRAAK

The crystal structure 4wfe[39] from OPM was used for TRAAK. 6 water behind the SF was preserved. The I159C and R284C mutations were introduced based on experimental results indicating that this disulfide bond can prevent the channel from closing.[39] In the previously reported WT simulation, a lipid can enter the pore from this fenestration site and possibly close the channel.[8] 246 POPC molecules were added using Charmm-GUI.[37,38] ACE and NME were added to cap the termini. The final system consisted of one channel, 246 POPC molecules, 27,973 water molecules, 403 K^+ ions, 389 Cl^- ions, corresponding to 0.8 m/L salt concentration.

426 4.1.3. MthK

427 For MthK the 3ldc[33] crystal structure was used. This structure was modified using the PyMOL
428 mutagenesis tool to perform H68S and C77V mutations to match the WT amino acid sequence.[40]
429 This structure was aligned using OPM. The Charmm-GUI Bilayer Builder was used to add ACE
430 and NME capping groups and to create the simulation box. Crystal water and potassium ions were
431 kept during this procedure. The final system contained 169 POPC molecules and 244 K^+ ions, 232
432 Cl^- and 16,900 water molecules, corresponding to 0.8 m/L salt concentration.

433

434 4.1.4. Kv1.2-2.1

435 The crystal structure of the Kv1.2-2.1 paddle chimera (2r9r[41]) from OPM was used. 8 water behind
436 SF was preserved. The pore and voltage-sensing domains (E144 to T417) were embedded in a
437 POPC membrane using Charmm-GUI. The functionally nonessential[42] tetramerization domain (T1)
438 and the regulatory β subunit were omitted. ACE and NME capping were added in Charmm-GUI.
439 The final system contained 313 POPC molecules and 460 K^+ ions, 452 Cl^- and 31,908 water
440 molecules, corresponding to 0.8 m/L salt concentration.

441

442 4.1.5. KcsA

443 A pre-equilibrated structure of the E71A mutant (that removes C-type inactivation), including 17
444 water molecules behind and on top of the SF, based on the 5vk6[43] crystal structure as used in
445 previous studies[44,45] was embedded in a POPC membrane using Charmm-GUI. ACE and NME
446 capping groups were used for the N- and C-terminus respectively. GLU118 and GLU120 were
447 protonated to mimic the state at pH 4. The final system contained 153 POPC molecules, 234 K^+
448 ions, 250 Cl^- and 16,196 water molecules, corresponding to 0.8 m/L salt concentration.

449

450 ## 4.2. Force field-specific parameters

451 ### 4.2.1. Charmm36m

452 For the Charmm36m[46] force field, Charmm lipid[47], Charmm TIP3P[48], and Charmm ions[49] were
453 used. A cutoff of 1.2 nm was used for van der Waals (vdW) interactions, and the forces were
454 switched smoothly to zero between 1.0 to 1.2 nm. The particle mesh Ewald (PME) method with a
455 1.2 nm cutoff was used for long-range electrostatic interactions.

456

457 ### 4.2.2. Amber14sb

458 For the Amber14sb[50] force field, lipid21[51], TIP3P water[52], and Joung and Cheatham ion
459 parameters[53] were used. A cutoff of 1.0 nm was used for van der Waals (vdW) interactions, and a
460 long-range analytical dispersion correction was applied to the energy and pressure. The PME
461 method with a 1.0 nm cutoff was used for long-range electrostatic interactions.

462

463 ### 4.2.3. Rescaled force fields

464 In one simulation box, the partial charges for all the charged residues including ions and charged
465 amino acids were adjusted with the same scaling factor, resulting in overall neutral simulation
466 systems. The partial charges for the charged amino acids were adjusted as follows. In Charmm36m
467 the partial charges of the charge group contributing to the net charge were multiplied by the
468 selected scaling factor. For example, in ASP the $-CH_2-CO_2$ group has a charge of -1. When charge
469 scaling is applied to ASP, the charge of the $-CH_2-CO_2$ group is scaled with the scaling factor (Fig.
470 S21). This approach could not be used in Amber, because the partial charges are also distributed
471 over the backbone atoms. Therefore, the scaled charges were obtained by taking a weighted
472 average (scaling factor as the weight) over the protonated and deprotonated charges (Fig. S21).
473 The deprotonated arginine, that was not available in the original amber14sb distribution, was
474 optimized at MP2/6-311G(d) using Gaussian 09 and RESP charge was fitted to HF/6-31G(d) with
475 antechamber.[54,55] All the partial charges used in this work at every scaling factors are provided in
476 the github repository:

477 https://github.com/deGrootLab/Charge_Scaling_in_Potassium_Channel_Simulations_paper/

4.2.4. Radius corrected vdW for charge scaled ion

The radius corrected vdW for the charge scaled ion was obtained and validated in the following 3 steps.

Step 1: Sigma optimization with grid search.

At each 0.05 charge from 1.00 (1.00, 0.95, 0.90 …) the sigma parameter of the ion decreased to the point when the radius of the first solvation shell reproduced the original radius in 1.00 charge. This sigma optimization was done by a grid search (a grid with (sigma, charge) pair). The setting and results of this grid search can be found in Fig. S8, and Fig. S9. The first peak in the ion-water oxygen RDF was used as the radius of the first solvation shell. Epsilon was kept the same as the original paper in the respective force field.[49,53] The sigma parameter between 0.05 charge (0.99, 0.98, 0.97, 0.96, 0.94 …) was linearly interpolated. The optimized vdW for K^+, Na^+, Cl^- is listed in Table S5.

In this step a simulation box with 2163 water molecules and 1 ion was used. Each (sigma, charge) pair on the grid was simulated for 40 ns, and trajectory was saved every 0.2 ps. Each grid (K^+, Na^+, Cl^-) was run in a Hamiltonian replica exchange simulation, and an exchange is attempted every 10 ps. RDF between ion and water oxygen is computed with "gmx rdf", using a bin width of 0.002 nm. The highest 7 points in the RDF were fitted with a Gaussian function (illustrated in Fig. S11). The same non-bonded settings for the corresponding force fields mentioned in Sections 4.2.1 and 4.2.2 were used.

Step 2: Solvation free energy validation

The ion solvation free energy calculation was performed using Gromacs 2022.5. The non-bonded parameters were set the same as previously mentioned in 4.2.1 and 4.2.2. Temperature was controlled by langevin integrator at 298 K and pressure was set at 1 bar using Parrinello-Rahman. The Coulomb interaction was gradually turned off in 10 lambda windows (0.0, 0.1, 0.2, 0.32, 0.44,

0.56, 0.68, 0.8, 0.9, 1.0, window 1-10), and vdw interaction was then turned off in the next 11 windows (0.0, 0.1, 0.2, 0.3, 0.4, 0.5, 0.6, 0.7, 0.8, 0.9, 1.0, window 10-20). HRE was used to speed up the sampling with an exchange attempt every 100 steps (0.2 ps). Each lambda window was simulated for 3 ns. The $\partial H/\partial \lambda$ and energy were saved every 2 ps. At least 1000 uncorrelated samples were recorded in each lambda window. "Alchemical-analysis" tool[56] was used and the reported value was estimated by the Multistate Bennett Acceptance Ratio (MBAR) method. A soft-core potential[57] was employed for the van der Waals interactions. The solvation free energy is shown in Fig. 4 and Fig. S10.

Step 3: RDF validation in dilute solution and 4M solution.

The RDF was validated under two conditions: (1) an infinitely diluted system, where the same simulation box as in step 1 was used, and (2) a 4M KCl solution, where the concentration matched that of the experiment.[58]

In the infinitely diluted system, each condition (charge with optimized sigma) was simulated for 100 ns and the trajectory is saved every 2 ps. The highest 7 points in the RDF were fitted with a Gaussian function (Fig. S11, Fig. S12). The radius is shown in Fig. 4 and Fig. S10.

A 4M system was constructed to compare with the neutron scattering experiment. The simulation box consisted of 6661 water, 120 K^+ ions, and 120 Cl^- ions. Each condition (charge with optimized sigma) was simulated for 20 ns, and the trajectory was saved every 1 ps. The experimental RDF was provided by the authors of the publication.[58] The RDF comparison is shown in Fig. S13.

All the initial structures, topology, and MD parameter files are provided in the github repository: https://github.com/deGrootLab/Charge_Scaling_in_Potassium_Channel_Simulations_paper/

532 ## 4.3. MD simulation

533 ### 4.3.1. Equilibration and general setting

534 Gromacs 2022.5 was used except for the charge-scaled HRE.[59,60] The initial structure was
535 minimized using the steepest descent until the maximum force was lower than 1000 kJ/(mol*nm).
536 100 ps of NVT with a harmonic restraint of 1000 kJ/(mol*nm^2) on all heavy atoms of protein and
537 POPC. The temperature in this equilibration was controlled by either the Berendsen (Charmm36m)
538 or v-rescale (Amber14sb) thermostat at 310 K. An additional 110 ns NPT equilibration was
539 performed to relax the membrane with harmonic restraints of 1000 kJ/(mol*nm^2) on all heavy
540 atoms of the protein. The temperature was controlled by either the Berendsen (Charmm36m) or
541 V-rescale (Amber14sb) thermostat at 310 K. The semi-isotropic pressure coupling was controlled
542 by the Berendsen barostat at 1 bar. The averaged box z dimension in the last 100 ns was used to
543 set the electric field. In the later production run, we switched to the Nose-Hoover (for Chamm36m)
544 or V-rescale (for Amber14sb) thermostat and the Parrinello-Rahman (for both Charmm36m and
545 Amber14sb) barostat. A time step of 2 fs was used, and bonds with Hydrogen atoms were
546 constrained by LINCS.[61]

547

548 ### 4.3.2. Non-equilibrium simulation under voltage

549 To simulate the channel under voltage, an electric field is applied.[62] In Charmm36m and
550 Amber14sb, the simulation was started after the equilibration, while in Amber14sb-S3, they were
551 started from the ensemble generated by HRE with randomly generated velocity at 310 K. For every
552 condition (including channel, force field, scaling factors, and voltage), 10 replicas of 500 ns were
553 performed.

554

555 When counting the K^+ current crossing the channel, we assume that 1 K^+ ion contributes to 1
556 elementary charge even if the partial charge is less than 1. The scaling of the partial charge is a
557 mean field treatment to approximate the polarization of the electron cloud between the nuclei, thus
558 the electric field (voltage) in the simulation is set the same for the 1.00 charge force field and a
559 charge scaled force field, and transporting 1 K^+ ion would generate the current of 1 elementary
560 charge regardless of the parameter.

4.3.3. Hamiltonian replica exchange (HRE)

The HRE simulations were performed on Gromacs 2021.7 with plumed 2.8.2.[63–65] Although Gromacs has its own HRE implementation, it only works with the free energy code and can only interpolate states using the lambda definition. The actual interpolation can be found in Gromacs documentation (https://manual.gromacs.org/2022.5/reference-manual/functions/free-energy-interactions.html).[59,60] In the Plumed Hamiltonian Replica Exchange (HRE) setup, each replica's Hamiltonian can be defined independently using separate topology files. We opted for Plumed HRE because this implementation allows every replica to have physically meaningful parameters, enabling us to assign distinct charges to each replica. Replica exchange is meaningful only in equilibrium conditions, so no voltage is applied. 36 replicas were set up with charge scaling factors decreasing from 1.00 to 0.65 in steps of 0.01, using the same simulation boxes as mentioned in the system preparation section. Every 100 MD steps (0.2 ps), an exchange attempt was tested. Each replica was simulated for 80 ns and the trajectory was saved every 20 ps. In our simulation practice, we found the HRE approach to be an efficient method to probe the scaling factor space. The conductance-scaling bar plot in Fig. 2(a) was obtained from 40 μs simulations with a scaling factor from 1.00 to 0.65 and a step of 0.05 (8 scaling factors, 10 replicas per scale, 500 ns every replica), while the SF state population plot in Fig. 2(d) was obtained from 2.88 μs simulation on the same simulation box with a scaling factor from 1.00 to 0.65 and a step of 0.01 (36 replicas, 80 ns each). Using HRE, with a fraction of the computation power, the high conductance parameters can be quickly located with fine resolution.

4.3.4. Comparison of solvation free energy with experiment

The solvation free energy calculated from the scaled ion cannot be directly compared with the experiment, because part of the energy from electric polarization (E_{ele}) is removed from the force field (E_{ff}) and treated in the mean field approximation. (Eq. 1) The actual solvation free energy can be splitted into 2 terms, ΔG_{nuc} which can be computed from MD solvation free energy calculation, and ΔG_{ele} which comes from the mean field approximation.

$$E_{total} = E_{ff} + E_{ele} \quad \text{(Eq. 1)}$$

$$\Delta G_{Exp} = \Delta G_{nuc} + \Delta G_{ele} \quad \text{(Eq. 2)}$$

Assuming the approximated medium between MD particles has a relative dielectric constant of ε_r, the ΔG_{ele} can be estimated with Born model (Eq. 3)

$$\Delta G = -\frac{N_A z^2 e^2}{8\pi\varepsilon_0 r_0}\left(1 - \frac{1}{\varepsilon_r}\right) \quad \text{(Eq. 3)}$$

N_A	Avogadro constant
z	charge of ion
e	elementary charge
ε_0	dielectric constant of vacuum
r_0	effective radius of ion in Born model

If we take scaling factor q as $1/\sqrt{\varepsilon_r}$, Eq. 3 becomes Eq. 4.

$$\Delta G_{ele} = -\frac{N_a z^2 e^2}{8\pi\varepsilon_0 r_0}(1 - q^2) \quad \text{(Eq. 4)}$$

The relative dielectric constant of water is significantly greater than 1 (ε_r for water = 78.4). We approximate the experimental solvation free energy using the Born model, as shown in Eq. 5.

$$\Delta G_{Exp} = -\frac{N_a z^2 e^2}{8\pi\varepsilon_0 r_0}\left(1 - \frac{1}{\varepsilon_{r_water}}\right) \approx -\frac{N_a z^2 e^2}{8\pi\varepsilon_0 r_0} \quad \text{(Eq. 5)}$$

So that the MD simulated solvation free energy should target the rest of the solvation free energy, which is Eq. 6.

$$\Delta G_{MD} = \Delta G_{Exp} - \Delta G_{ele} \qquad \text{(Eq. 6)}$$

$$\approx -\frac{N_a z^2 e^2}{8\pi\varepsilon_0 r_0} + \frac{N_a z^2 e^2}{8\pi\varepsilon_0 r_0}(1 - q^2)$$

$$= \Delta G_{Exp} * q^2$$

The comparing of experimental solvation free energy with ECC ion was discussed in several other references.[24,66]

4.4. Mechanism Graphs

The simulation was saved every 0.2 ps. The trajectory was discretized by the SF state. The rate between two states was defined as the inverse mean first passage time. All of the rates were first listed (every state pair, forward and backward), and the mechanism graph was progressively lumped from the state pair which had the fastest transition. If at least one of the forward or backward rates between a pair of states exceeded the cutoff rate, this pair of states would be lumped together. The cutoff rate when the lumping stopped is listed under each graph.

5. Acknowledgments

We would like to thank Youxing Jiang, Thomas Boulin, Dawon Kang, and Brad Rothberg for kindly sharing the experimental IV curves of NaK2K[1], TRAAK[30], and MthK[10]. We also thank Carter J. Wilson for providing the RESP charge of deprotonated arginine and Andrei Mironenko for providing the KcsA structure. R.d.V., W.K. and B.L.d.G. acknowledge funding from the Leibniz Collaborative Excellence Project "Ion Selectivity and Conduction Mechanism of Cation

Channels" K305/2020. W.K and B.L.d.G. acknowledge funding from the German Research Foundation (DFG) through FOR2518 'Dynion', Project P5.

6. Author contributions

W.K. and B.L.d.G. conceived and supervised the project. C.H. and R.d.V. performed all computational work and analyzed the data. C.H., R.d.V., W.K. and B.L.d.G. wrote the manuscript.

7. References

(1) Derebe, M. G.; Sauer, D. B.; Zeng, W.; Alam, A.; Shi, N.; Jiang, Y. Tuning the Ion Selectivity of Tetrameric Cation Channels by Changing the Number of Ion Binding Sites. *Proc. Natl. Acad. Sci.* **2011**, *108* (2), 598–602. https://doi.org/10.1073/pnas.1013636108.

(2) Zhou, Y.; Morais-Cabral, J. H.; Kaufman, A.; MacKinnon, R. Chemistry of Ion Coordination and Hydration Revealed by a K+ Channel–Fab Complex at 2.0 Å Resolution. *Nature* **2001**, *414* (6859), 43–48. https://doi.org/10.1038/35102009.

(3) Morais-Cabral, J. H.; Zhou, Y.; MacKinnon, R. Energetic Optimization of Ion Conduction Rate by the K+ Selectivity Filter. *Nature* **2001**, *414* (6859), 37–42. https://doi.org/10.1038/35102000.

(4) Langan, P. S.; Vandavasi, V. G.; Weiss, K. L.; Afonine, P. V.; el Omari, K.; Duman, R.; Wagner, A.; Coates, L. Anomalous X-Ray Diffraction Studies of Ion Transport in K+ Channels. *Nat. Commun.* **2018**, *9* (1), 4540. https://doi.org/10.1038/s41467-018-06957-w.

(5) Boiteux, C.; Posson, D. J.; Allen, T. W.; Nimigean, C. M. Selectivity Filter Ion Binding Affinity Determines Inactivation in a Potassium Channel. *Proc. Natl. Acad. Sci.* **2020**, *117* (47), 29968–29978. https://doi.org/doi:10.1073/pnas.2009624117.

(6) Köpfer, D. A.; Song, C.; Gruene, T.; Sheldrick, G. M.; Zachariae, U.; De Groot, B. L. Ion Permeation in K^+ Channels Occurs by Direct Coulomb Knock-On. *Science* **2014**, *346* (6207), 352–355. https://doi.org/10.1126/science.1254840.

(7) Kopec, W.; Köpfer, D. A.; Vickery, O. N.; Bondarenko, A. S.; Jansen, T. L. C.; de Groot, B. L.; Zachariae, U. Direct Knock-on of Desolvated Ions Governs Strict Ion Selectivity in K+ Channels. *Nat. Chem.* **2018**, *10* (8), 813–820. https://doi.org/10.1038/s41557-018-0105-9.

(8) Ocello, R.; Furini, S.; Lugli, F.; Recanatini, M.; Domene, C.; Masetti, M. Conduction and Gating Properties of the TRAAK Channel from Molecular Dynamics Simulations with Different Force Fields. *J. Chem. Inf. Model.* **2020**, *60* (12), 6532–6543. https://doi.org/10.1021/acs.jcim.0c01179.

(9) Lam, C. K.; De Groot, B. L. Ion Conduction Mechanisms in Potassium Channels Revealed by Permeation Cycles. *J. Chem. Theory Comput.* **2023**, *19* (9), 2574–2589. https://doi.org/10.1021/acs.jctc.3c00061.

(10) Kopec, W.; Thomson, A. S.; De Groot, B. L.; Rothberg, B. S. Interactions between Selectivity Filter and Pore Helix Control Filter Gating in the MthK Channel. *J. Gen. Physiol.* **2023**, *155* (8), e202213166. https://doi.org/10.1085/jgp.202213166.
(11) Mironenko, A.; Zachariae, U.; de Groot, B. L.; Kopec, W. The Persistent Question of Potassium Channel Permeation Mechanisms. *Ion Channels Intersect. Struct. Funct. Pharmacol.* **2021**, *433* (17), 167002. https://doi.org/10.1016/j.jmb.2021.167002.
(12) Jensen, M. Ø.; Borhani, D. W.; Lindorff-Larsen, K.; Maragakis, P.; Jogini, V.; Eastwood, M. P.; Dror, R. O.; Shaw, D. E. Principles of Conduction and Hydrophobic Gating in K^+ Channels. *Proc. Natl. Acad. Sci.* **2010**, *107* (13), 5833–5838. https://doi.org/10.1073/pnas.0911691107.
(13) Domene, C.; Ocello, R.; Masetti, M.; Furini, S. Ion Conduction Mechanism as a Fingerprint of Potassium Channels. *J. Am. Chem. Soc.* **2021**, *143* (31), 12181–12193. https://doi.org/10.1021/jacs.1c04802.
(14) Brennecke, J. T.; de Groot, B. L. Mechanism of Mechanosensitive Gating of the TREK-2 Potassium Channel. *Biophys. J.* **2018**, *114* (6), 1336–1343. https://doi.org/10.1016/j.bpj.2018.01.030.
(15) Guidoni, L.; Carloni, P. Potassium Permeation through the KcsA Channel: A Density Functional Study. *Biochim. Biophys. Acta BBA - Biomembr.* **2002**, *1563* (1–2), 1–6. https://doi.org/10.1016/S0005-2736(02)00349-8.
(16) Jing, Z.; Rackers, J. A.; Pratt, L. R.; Liu, C.; Rempe, S. B.; Ren, P. Thermodynamics of Ion Binding and Occupancy in Potassium Channels. *Chem. Sci.* **2021**, *12* (25), 8920–8930. https://doi.org/10.1039/D1SC01887F.
(17) Kirby, B. J.; Jungwirth, P. Charge Scaling Manifesto: A Way of Reconciling the Inherently Macroscopic and Microscopic Natures of Molecular Simulations. *J. Phys. Chem. Lett.* **2019**, *10* (23), 7531–7536. https://doi.org/10.1021/acs.jpclett.9b02652.
(18) E. Duboué-Dijon; M. Javanainen; P. Delcroix; P. Jungwirth; H. Martinez-Seara. A Practical Guide to Biologically Relevant Molecular Simulations with Charge Scaling for Electronic Polarization. *J. Chem. Phys.* **2020**, *153* (5), 050901. https://doi.org/10.1063/5.0017775.
(19) Melcr, J.; Ferreira, T. M.; Jungwirth, P.; Ollila, O. H. S. Improved Cation Binding to Lipid Bilayers with Negatively Charged POPS by Effective Inclusion of Electronic Polarization. *J. Chem. Theory Comput.* **2020**, *16* (1), 738–748. https://doi.org/10.1021/acs.jctc.9b00824.
(20) Melcr, J.; Martinez-Seara, H.; Nencini, R.; Kolafa, J.; Jungwirth, P.; Ollila, O. H. S. Accurate Binding of Sodium and Calcium to a POPC Bilayer by Effective Inclusion of Electronic Polarization. *J. Phys. Chem. B* **2018**, *122* (16), 4546–4557. https://doi.org/10.1021/acs.jpcb.7b12510.
(21) Nencini, R.; Tempra, C.; Biriukov, D.; Riopedre-Fernandez, M.; Cruces Chamorro, V.; Polák, J.; Mason, P. E.; Ondo, D.; Heyda, J.; Ollila, O. H. S.; Jungwirth, P.; Javanainen, M.; Martinez-Seara, H. Effective Inclusion of Electronic Polarization Improves the Description of Electrostatic Interactions: The prosECCo75 Biomolecular Force Field. *J. Chem. Theory Comput.* **2024**, *20* (17), 7546–7559. https://doi.org/10.1021/acs.jctc.4c00743.
(22) Laage, D.; Stirnemann, G. Effect of Ions on Water Dynamics in Dilute and Concentrated Aqueous Salt Solutions. *J. Phys. Chem. B* **2019**, *123* (15), 3312–3324. https://doi.org/10.1021/acs.jpcb.9b01053.
(23) Wilson, C. J.; Gapsys, V.; De Groot, B. L. Improving pKa Prediction Accuracy with Reparametrized Force Fields and Free Energy Calculations. January 9, 2025. https://doi.org/10.26434/chemrxiv-2024-btnq5-v2.

(24) Leontyev, I. V.; Stuchebrukhov, A. A. Electronic Continuum Model for Molecular Dynamics Simulations of Biological Molecules. *J. Chem. Theory Comput.* **2010**, *6* (5), 1498–1508. https://doi.org/10.1021/ct9005807.
(25) Lee, B.; White, K. I.; Socolich, M.; Klureza, M. A.; Henning, R.; Srajer, V.; Ranganathan, R.; Hekstra, D. R. Direct Visualization of Electric-Field-Stimulated Ion Conduction in a Potassium Channel. *Cell* **2025**, *188* (1), 77-88.e15. https://doi.org/10.1016/j.cell.2024.12.006.
(26) Bernèche, S.; Roux, B. Energetics of Ion Conduction through the K+ Channel. *Nature* **2001**, *414* (6859), 73–77. https://doi.org/10.1038/35102067.
(27) Jensen, M. Ø.; Jogini, V.; Eastwood, M. P.; Shaw, D. E. Atomic-Level Simulation of Current–Voltage Relationships in Single-File Ion Channels. *J. Gen. Physiol.* **2013**, *141* (5), 619–632. https://doi.org/10.1085/jgp.201210820.
(28) Abdul Kadir, L.; Stacey, M.; Barrett-Jolley, R. Emerging Roles of the Membrane Potential: Action Beyond the Action Potential. *Front. Physiol.* **2018**, *9*, 1661. https://doi.org/10.3389/fphys.2018.01661.
(29) Lazzari-Dean, J. R.; Gest, A. M. M.; Miller, E. W. Measuring Absolute Membrane Potential Across Space and Time. *Annu. Rev. Biophys.* **2021**, *50* (1), 447–468. https://doi.org/10.1146/annurev-biophys-062920-063555.
(30) Ben Soussia, I.; El Mouridi, S.; Kang, D.; Leclercq-Blondel, A.; Khoubza, L.; Tardy, P.; Zariohi, N.; Gendrel, M.; Lesage, F.; Kim, E.-J.; Bichet, D.; Andrini, O.; Boulin, T. Mutation of a Single Residue Promotes Gating of Vertebrate and Invertebrate Two-Pore Domain Potassium Channels. *Nat. Commun.* **2019**, *10* (1), 787. https://doi.org/10.1038/s41467-019-08710-3.
(31) Miranda, W. E.; DeMarco, K. R.; Guo, J.; Duff, H. J.; Vorobyov, I.; Clancy, C. E.; Noskov, S. Yu. Selectivity Filter Modalities and Rapid Inactivation of the hERG1 Channel. *Proc. Natl. Acad. Sci.* **2020**, *117* (6), 2795–2804. https://doi.org/10.1073/pnas.1909196117.
(32) Sumikama, T.; Oiki, S. Digitalized K^+ Occupancy in the Nanocavity Holds and Releases Queues of K^+ in a Channel. *J. Am. Chem. Soc.* **2016**, *138* (32), 10284–10292. https://doi.org/10.1021/jacs.6b05270.
(33) Ye, S.; Li, Y.; Jiang, Y. Novel Insights into K+ Selectivity from High-Resolution Structures of an Open K+ Channel Pore. *Nat. Struct. Mol. Biol.* **2010**, *17* (8), 1019–1023. https://doi.org/10.1038/nsmb.1865.
(34) Atkins, P.; De Paula, J.; Keeler, J. *Atkins' Physical Chemistry*, 11th ed.; Oxford University Press: London, England, 2017.
(35) Lomize, M. A.; Pogozheva, I. D.; Joo, H.; Mosberg, H. I.; Lomize, A. L. OPM Database and PPM Web Server: Resources for Positioning of Proteins in Membranes. *Nucleic Acids Res.* **2012**, *40* (D1), D370–D376. https://doi.org/10.1093/nar/gkr703.
(36) Sauer, D. B.; Zeng, W.; Canty, J.; Lam, Y.; Jiang, Y. Sodium and Potassium Competition in Potassium-Selective and Non-Selective Channels. *Nat. Commun.* **2013**, *4* (1), 2721. https://doi.org/10.1038/ncomms3721.
(37) Jo, S.; Lim, J. B.; Klauda, J. B.; Im, W. CHARMM-GUI Membrane Builder for Mixed Bilayers and Its Application to Yeast Membranes. *Biophys. J.* **2009**, *97* (1), 50–58. https://doi.org/10.1016/j.bpj.2009.04.013.
(38) Jo, S.; Kim, T.; Iyer, V. G.; Im, W. CHARMM-GUI: A Web-based Graphical User Interface for CHARMM. *J. Comput. Chem.* **2008**, *29* (11), 1859–1865. https://doi.org/10.1002/jcc.20945.

(39) Brohawn, S. G.; Campbell, E. B.; MacKinnon, R. Physical Mechanism for Gating and Mechanosensitivity of the Human TRAAK K+ Channel. *Nature* **2014**, *516* (7529), 126–130. https://doi.org/10.1038/nature14013.
(40) The PyMOL Molecular Graphics System, Version 2.5.4 Schrödinger, LLC.
(41) Long, S. B.; Tao, X.; Campbell, E. B.; MacKinnon, R. Atomic Structure of a Voltage-Dependent K+ Channel in a Lipid Membrane-like Environment. *Nature* **2007**, *450* (7168), 376–382. https://doi.org/10.1038/nature06265.
(42) Miller, C.; Kobertz, W. R. K+ Channels Lacking the "tetramerization" Domain: Implications for Pore Structure. *Nat. Struct. Biol.* **1999**, *6* (12), 1122–1125. https://doi.org/10.1038/70061.
(43) Cuello, L. G.; Cortes, D. M.; Perozo, E. The Gating Cycle of a K+ Channel at Atomic Resolution. *eLife* **2017**, *6*, e28032. https://doi.org/10.7554/eLife.28032.
(44) Mironenko, A.; De Groot, B. L.; Kopec, W. Selectivity Filter Mutations Shift Ion Permeation Mechanism in Potassium Channels. *PNAS Nexus* **2024**, *3* (7), pgae272. https://doi.org/10.1093/pnasnexus/pgae272.
(45) Pérez-Conesa, S.; Delemotte, L. Free Energy Landscapes of KcsA Inactivation. July 4, 2023. https://doi.org/10.7554/eLife.88403.1.
(46) Huang, J.; Rauscher, S.; Nawrocki, G.; Ran, T.; Feig, M.; de Groot, B. L.; Grubmüller, H.; MacKerell, A. D. CHARMM36m: An Improved Force Field for Folded and Intrinsically Disordered Proteins. *Nat. Methods* **2017**, *14* (1), 71–73. https://doi.org/10.1038/nmeth.4067.
(47) Klauda, J. B.; Venable, R. M.; Freites, J. A.; O'Connor, J. W.; Tobias, D. J.; Mondragon-Ramirez, C.; Vorobyov, I.; MacKerell, A. D.; Pastor, R. W. Update of the CHARMM All-Atom Additive Force Field for Lipids: Validation on Six Lipid Types. *J. Phys. Chem. B* **2010**, *114* (23), 7830–7843. https://doi.org/10.1021/jp101759q.
(48) MacKerell, A. D.; Bashford, D.; Bellott, M.; Dunbrack, R. L.; Evanseck, J. D.; Field, M. J.; Fischer, S.; Gao, J.; Guo, H.; Ha, S.; Joseph-McCarthy, D.; Kuchnir, L.; Kuczera, K.; Lau, F. T. K.; Mattos, C.; Michnick, S.; Ngo, T.; Nguyen, D. T.; Prodhom, B.; Reiher, W. E.; Roux, B.; Schlenkrich, M.; Smith, J. C.; Stote, R.; Straub, J.; Watanabe, M.; Wiórkiewicz-Kuczera, J.; Yin, D.; Karplus, M. All-Atom Empirical Potential for Molecular Modeling and Dynamics Studies of Proteins. *J. Phys. Chem. B* **1998**, *102* (18), 3586–3616. https://doi.org/10.1021/jp973084f.
(49) Beglov, D.; Roux, B. Finite Representation of an Infinite Bulk System: Solvent Boundary Potential for Computer Simulations. *J. Chem. Phys.* **1994**, *100* (12), 9050–9063. https://doi.org/10.1063/1.466711.
(50) Maier, J. A.; Martinez, C.; Kasavajhala, K.; Wickstrom, L.; Hauser, K. E.; Simmerling, C. ff14SB: Improving the Accuracy of Protein Side Chain and Backbone Parameters from ff99SB. *J. Chem. Theory Comput.* **2015**, *11* (8), 3696–3713. https://doi.org/10.1021/acs.jctc.5b00255.
(51) Dickson, C. J.; Walker, R. C.; Gould, I. R. Lipid21: Complex Lipid Membrane Simulations with AMBER. *J. Chem. Theory Comput.* **2022**, *18* (3), 1726–1736. https://doi.org/10.1021/acs.jctc.1c01217.
(52) Jorgensen, W. L.; Chandrasekhar, J.; Madura, J. D.; Impey, R. W.; Klein, M. L. Comparison of Simple Potential Functions for Simulating Liquid Water. *J. Chem. Phys.* **1983**, *79* (2), 926–935. https://doi.org/10.1063/1.445869.
(53) Joung, I. S.; Cheatham, T. E. Determination of Alkali and Halide Monovalent Ion Parameters for Use in Explicitly Solvated Biomolecular Simulations. *J. Phys. Chem. B* **2008**, *112* (30), 9020–9041. https://doi.org/10.1021/jp8001614.

(54) Wang, J.; Wang, W.; Kollman, P. A.; Case, D. A. Automatic Atom Type and Bond Type Perception in Molecular Mechanical Calculations. *J. Mol. Graph. Model.* **2006**, *25* (2), 247–260. https://doi.org/10.1016/j.jmgm.2005.12.005.

(55) Frisch, M. J.; Trucks, G. W.; Schlegel, H. B.; Scuseria, G. E.; Robb, M. A.; Cheeseman, J. R.; Scalmani, G.; Barone, V.; Mennucci, B.; Petersson, G. A.; Nakatsuji, H.; Caricato, M.; Li, X.; Hratchian, H. P.; Izmaylov, A. F.; Bloino, J.; Zheng, G.; Sonnenberg, J. L.; Hada, M.; Ehara, M.; Toyota, K.; Fukuda, R.; Hasegawa, J.; Ishida, M.; Nakajima, T.; Honda, Y.; Kitao, O.; Nakai, H.; Vreven, T.; Montgomery, J. A.; Peralta, J. E.; Ogliaro, F.; Bearpark, M.; Heyd, J. J.; Brothers, E.; Kudin, K. N.; Staroverov, V. N.; Kobayashi, R.; Normand, J.; Raghavachari, K.; Rendell, A.; Burant, J. C.; Iyengar, S. S.; Tomasi, J.; Cossi, M.; Rega, N.; Millam, M. J.; Klene, M.; Knox, J. E.; Cross, J. B.; Bakken, V.; Adamo, C.; Jaramillo, J.; Gomperts, R.; Stratmann, R. E.; Yazyev, O.; Austin, A. J.; Cammi, R.; Pomelli, C.; Ochterski, J. W.; Martin, R. L.; Morokuma, K.; Zakrzewski, V. G.; Voth, G. A.; Salvador, P.; Dannenberg, J. J.; Dapprich, S.; Daniels, A. D.; Farkas, Ö.; Foresman, J. B.; Ortiz, J. V.; Cioslowski, J.; Fox, D. J. Gaussian 09 Revision D.01.

(56) Klimovich, P. V.; Shirts, M. R.; Mobley, D. L. Guidelines for the Analysis of Free Energy Calculations. *J. Comput. Aided Mol. Des.* **2015**, *29* (5), 397–411. https://doi.org/10.1007/s10822-015-9840-9.

(57) Beutler, T. C.; Mark, A. E.; Van Schaik, R. C.; Gerber, P. R.; Van Gunsteren, W. F. Avoiding Singularities and Numerical Instabilities in Free Energy Calculations Based on Molecular Simulations. *Chem. Phys. Lett.* **1994**, *222* (6), 529–539. https://doi.org/10.1016/0009-2614(94)00397-1.

(58) Mason, P. E.; Tavagnacco, L.; Saboungi, M.-L.; Hansen, T.; Fischer, H. E.; Neilson, G. W.; Ichiye, T.; Brady, J. W. Molecular Dynamics and Neutron Scattering Studies of Potassium Chloride in Aqueous Solution. *J. Phys. Chem. B* **2019**, *123* (50), 10807–10813. https://doi.org/10.1021/acs.jpcb.9b08422.

(59) Bauer, P.; Hess, B.; Lindahl, E. GROMACS 2022.5 Manual. **2023**. https://doi.org/10.5281/ZENODO.7586765.

(60) Abraham, M. J.; Murtola, T.; Schulz, R.; Páll, S.; Smith, J. C.; Hess, B.; Lindahl, E. GROMACS: High Performance Molecular Simulations through Multi-Level Parallelism from Laptops to Supercomputers. *SoftwareX* **2015**, *1–2*, 19–25. https://doi.org/10.1016/j.softx.2015.06.001.

(61) Hess, B.; Bekker, H.; Berendsen, H. J. C.; Fraaije, J. G. E. M. LINCS: A Linear Constraint Solver for Molecular Simulations. *J. Comput. Chem.* **1997**, *18* (12), 1463–1472. https://doi.org/10.1002/(SICI)1096-987X(199709)18:12<1463::AID-JCC4>3.0.CO;2-H.

(62) Roux, B. The Membrane Potential and Its Representation by a Constant Electric Field in Computer Simulations. *Biophys. J.* **2008**, *95* (9), 4205–4216. https://doi.org/10.1529/biophysj.108.136499.

(63) The PLUMED consortium. Promoting Transparency and Reproducibility in Enhanced Molecular Simulations. *Nat. Methods* **2019**, *16* (8), 670–673. https://doi.org/10.1038/s41592-019-0506-8.

(64) Tribello, G. A.; Bonomi, M.; Branduardi, D.; Camilloni, C.; Bussi, G. PLUMED 2: New Feathers for an Old Bird. *Comput. Phys. Commun.* **2014**, *185* (2), 604–613. https://doi.org/10.1016/j.cpc.2013.09.018.

(65) Bonomi, M.; Branduardi, D.; Bussi, G.; Camilloni, C.; Provasi, D.; Raiteri, P.; Donadio, D.; Marinelli, F.; Pietrucci, F.; Broglia, R. A.; Parrinello, M. PLUMED: A Portable Plugin for

Free-Energy Calculations with Molecular Dynamics. *Comput. Phys. Commun.* **2009**, *180* (10), 1961–1972. https://doi.org/10.1016/j.cpc.2009.05.011.

(66) Leontyev, I.; Stuchebrukhov, A. Accounting for Electronic Polarization in Non-Polarizable Force Fields. *Phys. Chem. Chem. Phys.* **2011**, *13* (7), 2613–2626. https://doi.org/10.1039/C0CP01971B.

(67) Marcus, Y. Ionic Radii in Aqueous Solutions. *Chem. Rev.* **1988**, *88* (8), 1475–1498. https://doi.org/10.1021/cr00090a003.

(68) Schmid, R.; Miah, A. M.; Sapunov, V. N. A New Table of the Thermodynamic Quantities of Ionic Hydration: Values and Some Applications (Enthalpy–Entropy Compensation and Born Radii). *Phys. Chem. Chem. Phys.* **2000**, *2* (1), 97–102. https://doi.org/10.1039/A907160A.

Figures

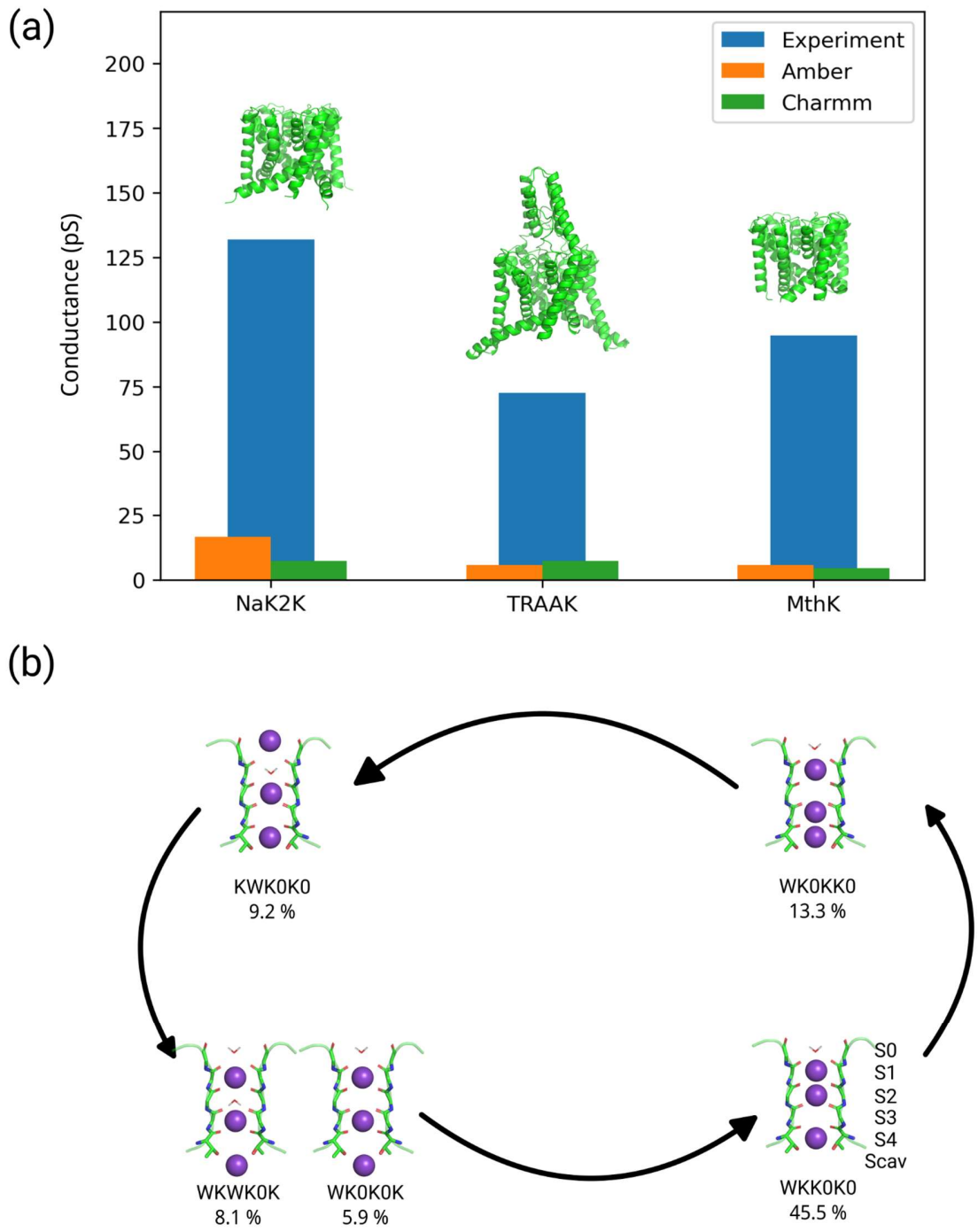

Figure 1. Main features of K^+ permeation through K^+ channels in MD simulations with traditional force fields. (a) Comparison of experimental conductances[1,10,30] and MD simulated conductances in 3

channels (NaK2K, TRAAK, MthK), with 2 force fields (Charmm36m and Amber14sb), at +100 mV. **(b)** A schematic mechanism of ion permeation in NaK2K in MD simulations using Charmm36m at +100 mV. Trajectories were discretized based on the number of K^+ ions in positions S0-SCav. The SF occupancy is represented using a 6-letter code showing the occupancy at binding sites S0 to SCav: 'K' for a K^+ ion, 'W' for water, and '0' for an unoccupied site. Populations of SF states are expressed as percentages, with WKK0K0, WK0KK0, KWK0K0, WKWK0K, and WK0K0K being the only states exceeding a 5% population.

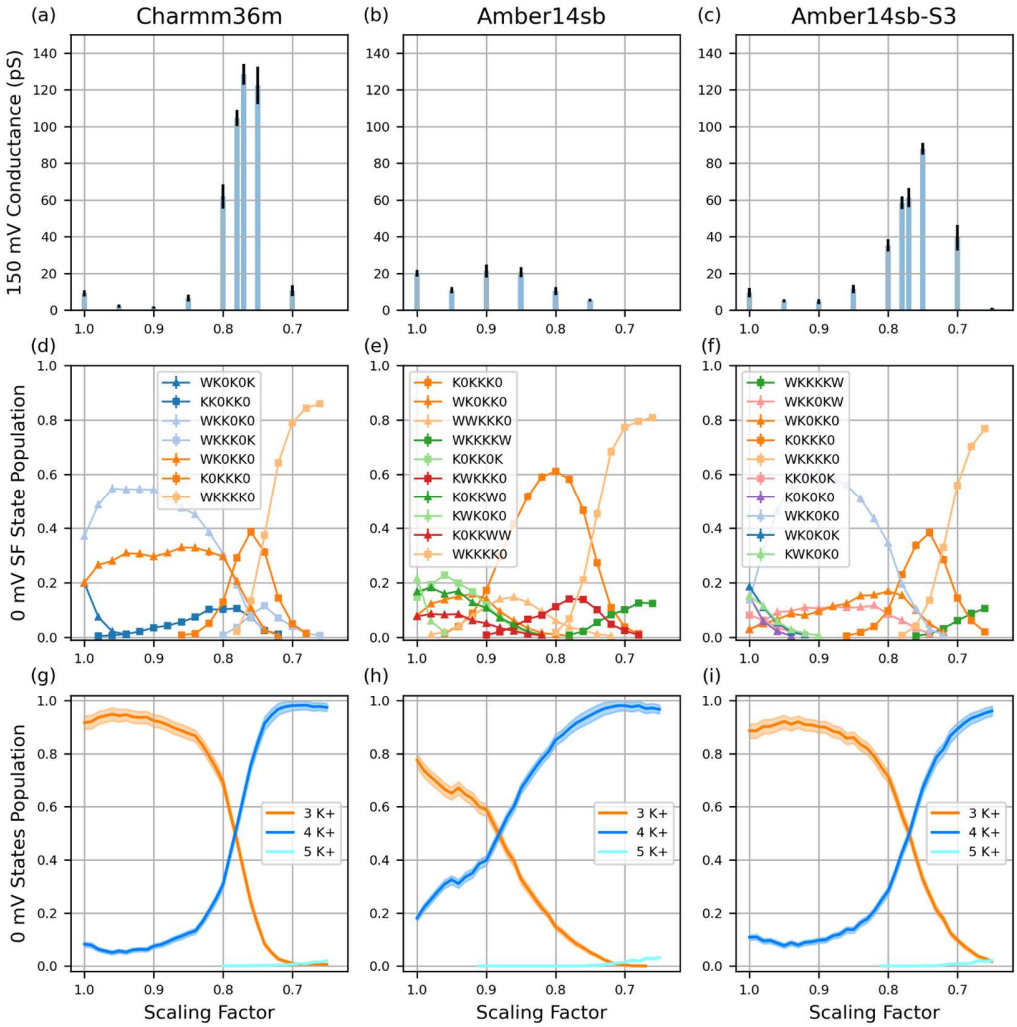

Figure 2. Charge scaling has a major impact on ion permeation characteristics in the NaK2K channel. (**a-c**) Average conductances at different scaling factors in MD simulations using Charmm36m, Amber14sb, and Amber14sb-S3 (see text for explanation) force fields under +150 mV in NaK2K. The error bar is the standard error of the mean (N=10). **(d-f)** Equilibrated populations of the SF states recorded in HRE in NaK2K, using a 6-letter code showing the occupancy at binding sites S0 to Scav: 'K' for a K^+ ion, 'W' for water, and '0' for an unoccupied site. For clarity, only the even replicas are plotted (replica 0, 2, 4 etc at scale 1.00, 0.98, 0.96 etc). The odd replicas are not shown (replica 1, 3, 5 etc at scale 0.99, 0.97, 0.95 etc). **(g-i)** Ion occupation state distribution from HRE simulation, the states with the same number of ions in the SF are summed together. In (d-i) The error bar is the 95% confidence interval when bootstrapping frames.

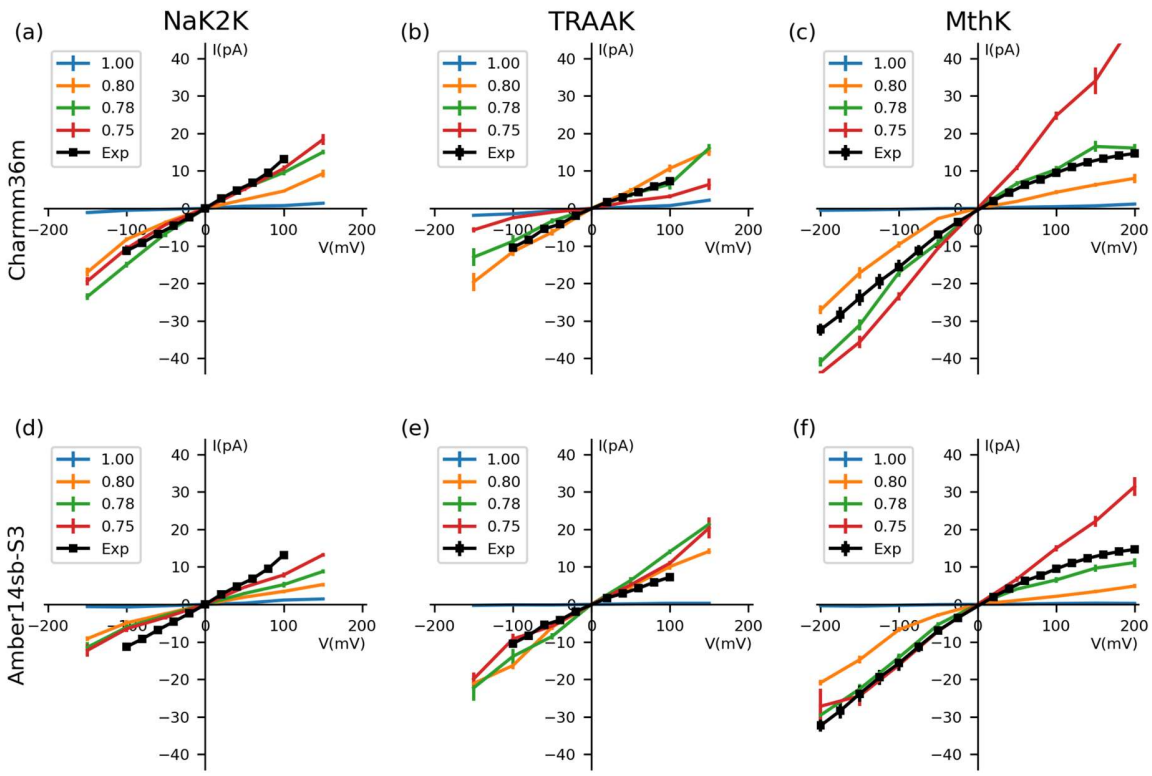

Figure 3. Simulated full current-voltage (I-V) curves for NaK2K, TRAAK, and MthK channels at different scaling factors. (a-c) Simulated I-V curves with Charmm36m. **(d-f)** Simulated I-V curve with Amber14sb-S3. MD simulations were performed at ± 50 mV, ± 100 mV, ± 150 mV, ± 200 mV (if the experiment data covered ± 200 mV). The experimental data are shown in black and were provided by the authors of respective publications.[1,10,30] Simulated data are shown in colors for different scaling factors. The error bar is the standard error of the mean in all cases. The digital data can be found in the SI file.

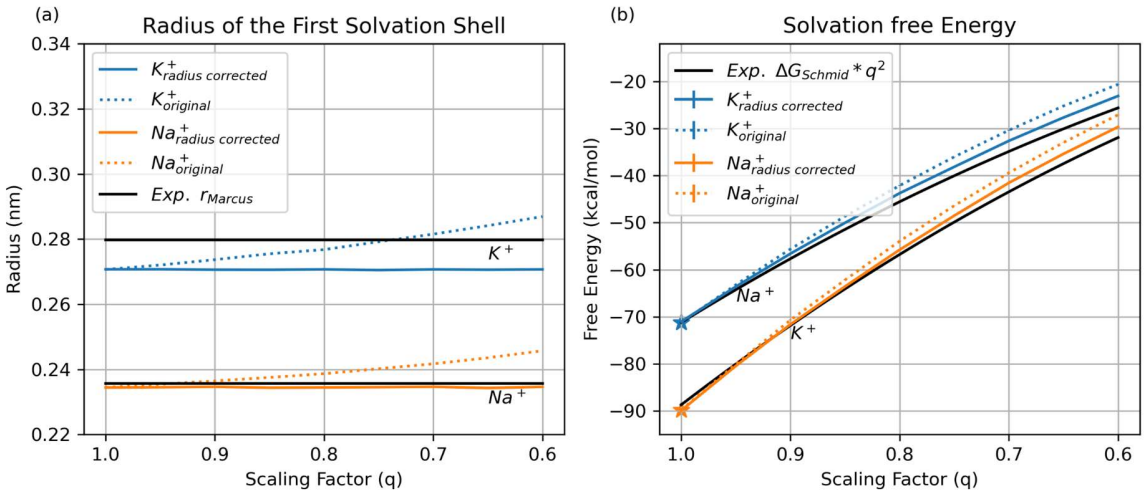

Figure 4. Comparison of the radius corrected LJ parameters for ECC ion in this work (solid line) and the original vdW (dotted line) in Charmm36m. (a) The radius of the first solvation shell for K^+ and Na^+ with two sets of LJ parameters, compared to the experimental value.[67] (b) The solvation free energy for K^+ and Na^+ with two sets of vdW parameters. The experimental solvation free energy from Schimdt et al.[68] was scaled at each scaling factor, following the Born model (see Methods for details). The experiment value was from the respective references. The vdW parameters at 1.0 scale were taken from the original force field. The same plot for Amber14sb is shown in Fig. S10.

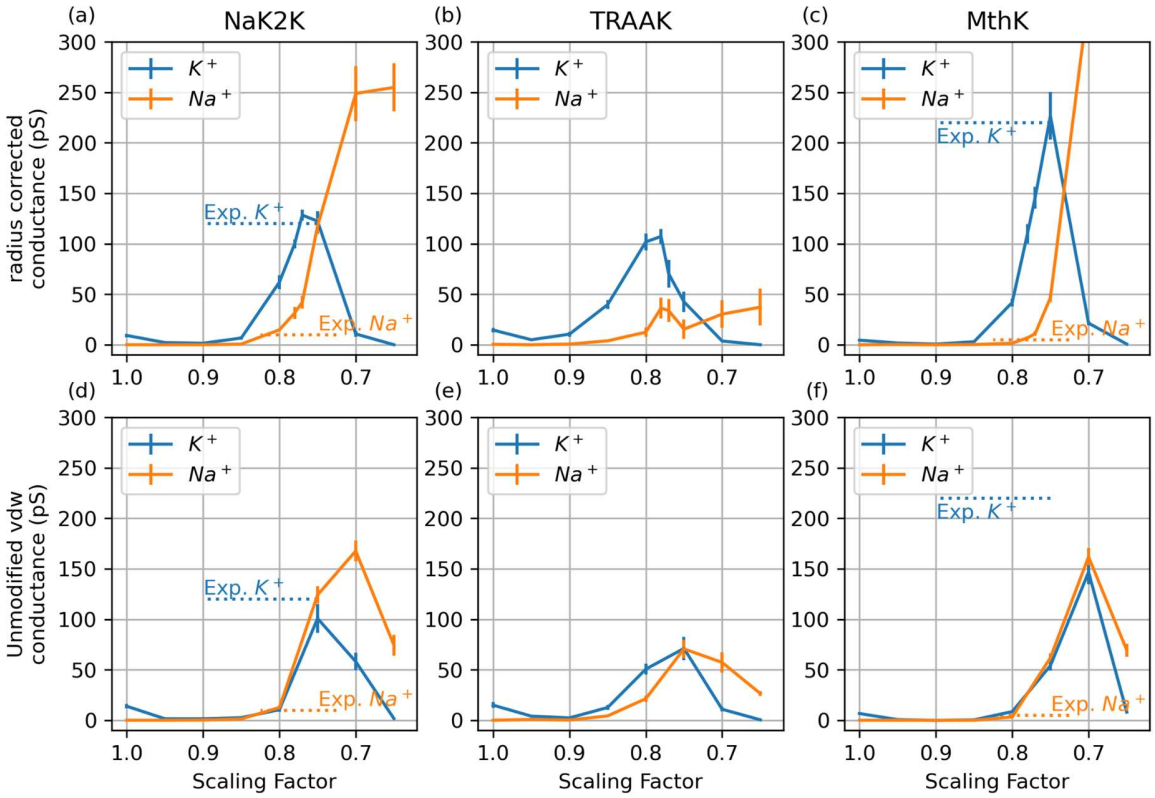

Figure 5. K^+ and Na^+ conductance with two treatments of LJ parameters in Charmm36m. (a-c) Simulated conductances with our newly developed radius-corrected LJ parameters for ECC ions. **(d-f)** Simulated conductance with unmodified LJ parameters in Charmm36m. All simulations were performed under +150 mV voltage. The analogous plot for Amber14-S3 is in Fig S14. The experimental values were taken from the respective references.[1,33]

Table 1. K^+/ Na^+ conductance ratio at 0.78 scale, at +150 mV

	NaK2K	TRAAK	MthK
Charmm36m	3.3	2.5	16.1
Amber14sb-S3	2.5	7.7	8.4

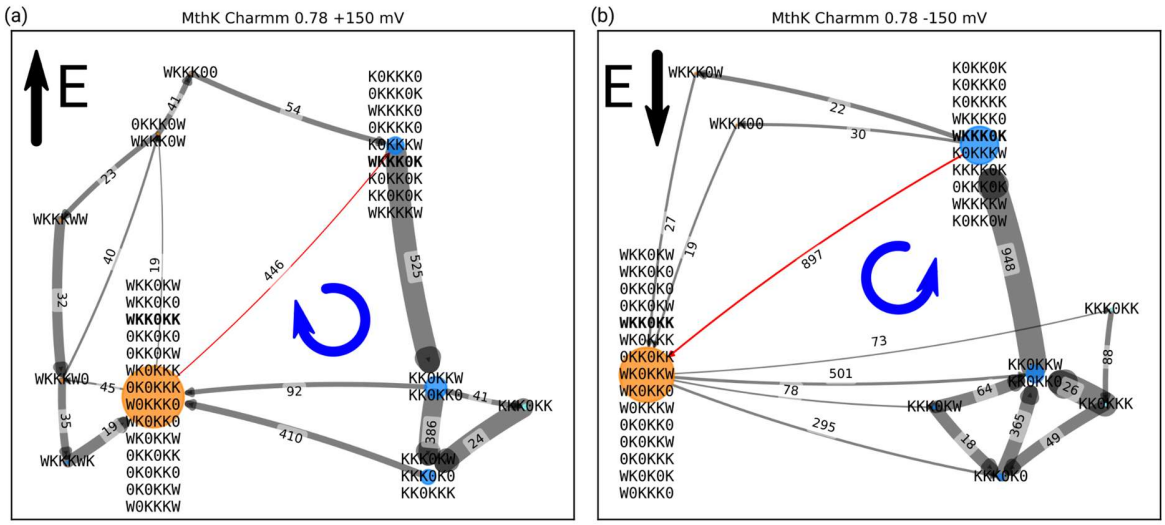

Figure 6. The mechanism graph from simulations of MthK in Charmm36m with 0.78 scaling under +150 mV or -150 mV. 515 (a) and 970 (b) permeation events were observed in 500 ns x 10 replica simulations at each voltage, respectively. The numbers shown by the edges are the net flux. The thickness of the edge (arrow) is proportional to the rate (defined as the inverse of the mean first passage time). The size of a node corresponds to the overall population of all states in this node. Nodes with 4 K^+ ions in SF are shown in orange, and nodes with 3 K^+ ions in SF are shown in blue. In panel (a), states A and B are lumped together when rate exceeds 125.0 ns^{-1}, similarly, in panel (b), they are lumped when this product exceeds 180.0 ns^{-1}. The rate-limiting step is marked in red. The exact flux and rate between all state pairs in the rate limiting step can be found in Table S4. The state pair WKKK0K-WKK0KK contributes to more than 85% of the net flux, and is identified as the rate-limiting step without lumping.

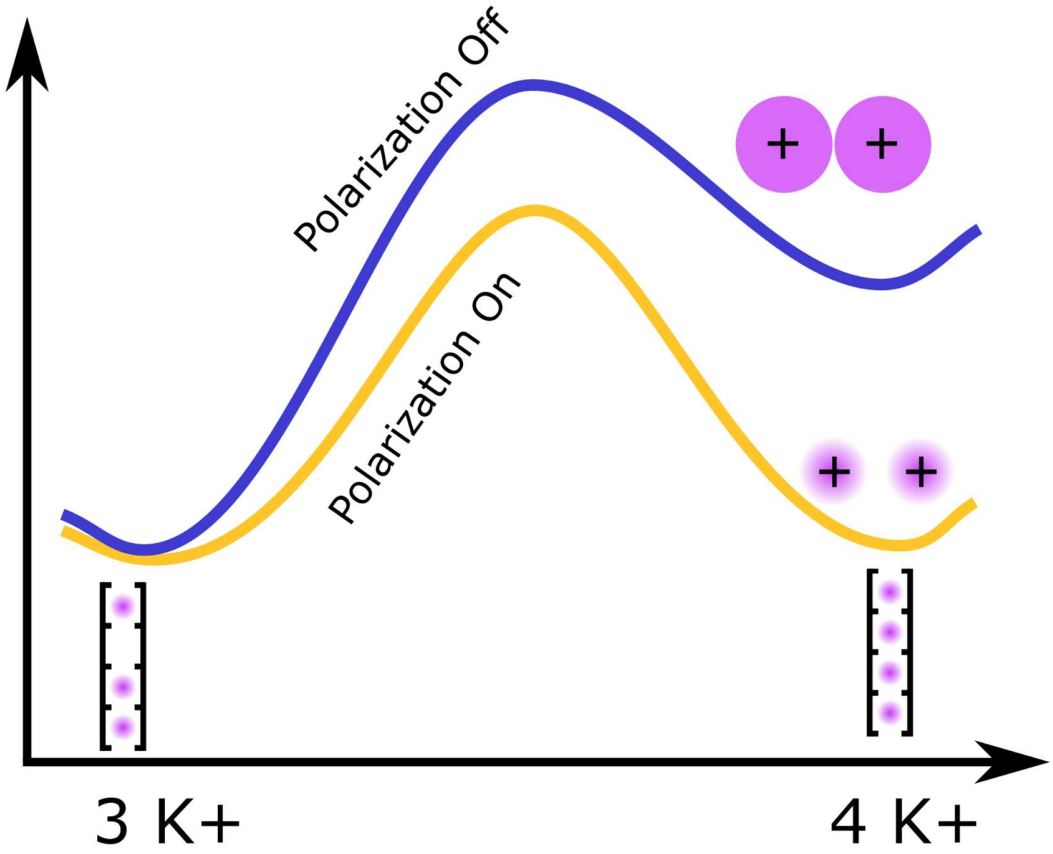

Figure 7. Schematic energy landscape between 3 and 4 K^+ states with/without polarization. Only 1 SF state is drawn for 3 and 4 K^+ states, and in reality, multiple 3 K^+ and multiple 4 K^+ states are visited. When the ECC polarization is introduced, the dominating effect is a decreased ion-ion repulsion, leading to more ion-ion contacts and fully ion filled filters, as well as a reduced barrier to form such contacts, and thus a more efficient knock-on permeation.